ROYAL SOCIETY
OF CHEMISTRY

PAPER

Check for updates

Hydroxylamine intermediate governs selectivity in nitrite hydrogenation on Pd-based catalysts for sustainable water treatment

Janek Betting, [ID] [a] Yardthip Preedawichitkun, [b] Tawan Sooknoi, [ID] [b] Leon Lefferts [ID] *[a] and Jimmy A. Faria Albanese [ID] *[a]

Catalytic hydrogenation of nitrate (NO_3^-) and nitrite (NO_2^-) is a promising route for drinking water purification and rebalancing the global nitrogen cycle. Recently, hydroxylamine (NH_2OH) was detected as a persistent reaction intermediate although ammonium (NH_4^+) and dinitrogen (N_2) were assumed to be the only significant reaction products for several decades. In this work, we systematically investigate NO_2^- hydrogenation over Pd/Al_2O_3 and $SnPd/Al_2O_3$ while explicitly quantifying NH_2OH under various conditions, including changes in H_2 partial pressure, the initial NO_2^- concentration, and reaction temperature, and through co-feeding of NH_2OH. We reveal that NH_4^+ selectivity depends strongly on the NO_2^- conversion level, reflecting shifts in surface coverages as the reaction progresses. Suppression of both NH_2OH and NH_4^+ formation is only achievable under H_2-deficient conditions, though this comes at the expense of lower overall hydrogenation activity. Elevated temperatures enhance NH_2OH decomposition and thereby promote NH_4^+ formation, while leaving N_2 selectivity largely unaffected. Co-feeding experiments further show that externally introduced NH_2OH does not influence the NO_2^- hydrogenation rate. We critically reviewed prior mechanistic studies on NO_2^- hydrogenation and propose a refined Langmuir–Hinshelwood scheme that explicitly incorporates NH_2OH as a desorbed intermediate. This work highlights the importance of NH_2OH in the reaction network and underscores the need to include it in the assessment of the reaction selectivity.

1 Introduction

Nitrate (NO_3^-) and nitrite (NO_2^-) are water contaminants that pose a serious threat to both human health and aquatic ecosystems if not properly controlled. Although these species are natural components of the biogeochemical nitrogen cycle, the excessive use of nitrogen-based fertilizers has severely disrupted this balance in recent decades.[1–4] As a consequence, nitrogen nutrient levels have risen in inland, coastal, and marine waters, driving eutrophication.[5] Eutrophication negatively impacts entire ecosystems by reducing biodiversity of animals and plants. In addition, elevated nitrate and nitrite concentrations can directly affect human health. When present in drinking water, these species may cause methemoglobinemia—commonly known as "blue baby syndrome"[6] and have, therefore, strict limits (50 and 5 mg L^{-1}, respectively).[7]

Catalytic nitrate and nitrite reduction has emerged as a promising technology to convert these species into harmless dinitrogen (N_2).[8] In contrast to alternative remediation methods such as reverse osmosis, ion exchange, or electrodialysis, catalytic reduction degrades the contaminants rather than concentrating them into waste brines.[8] Nitrate is first reduced to nitrite, which is then further hydrogenated to N_2. In this reaction network, the hydrogenation of nitrate to nitrite is the rate determining step (RDS) and requires a bimetallic catalyst (*e.g.* Sn–Pd, Cu–Pd, or In–Pd), while the subsequent nitrite hydrogenation can be catalyzed by Pd alone.[9–12]

$$NO_3^- + H_2 \rightarrow NO_2^- + H_2O \quad (1)$$

$$2\,NO_2^- + 3H_2 + 2H^+ \rightarrow N_2 + 4H_2O \quad (2)$$
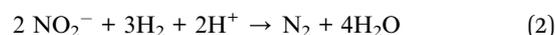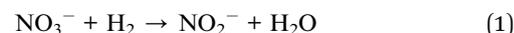
The main challenge for application remains the formation of ammonium (NH_4^+), which follows even stricter regulations (0.5 mg L^{-1}).[13]

$$NO_2^- + 3H_2 + 2H^+ \rightarrow NH_4^+ + 2H_2O \quad (3)$$

While the formation of NH_2OH in electro- and photocatalytic NO_3^- and NO_2^- reduction has been reported in the past,[14–16] its presence in thermo-catalytic conversion was only reported very recently. The results showed that hydroxylamine (NH_2OH) is an

[a]Catalytic Processes and Materials Group, Department for Chemical Engineering, Faculty of Science and Technology, MESA+ Institute for Nanotechnology, University of Twente, Enschede 7500 AE, The Netherlands. E-mail: j.a.fariaalbanese@utwente.nl
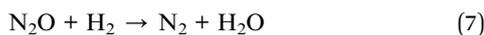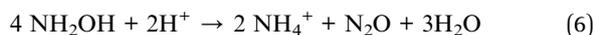*[b]Department of Chemisty, Faculty of Science, King Mongkut's Institute of Technology Ladkrabang, Chalongkrung Road, Ladkrabang, Bangkok 10520, Thailand*

omnipresent and long-lasting reaction intermediate under various reaction conditions on several different catalysts (eqn (4)).[17] Until then, a pervasive assumption in the field was that N_2 and ammonium (NH_4^+) were the only relevant reaction products of thermocatalytic NO_3^- and NO_2^- hydrogenation under relevant reaction conditions for drinking water purification.[8–12,18–22]

$$NO_2^- + 2H_2 + H^+ \rightarrow NH_2OH + H_2O \qquad (4)$$

Hydroxylamine is highly toxic and harmful for water bodies[23] and therefore represents a major challenge for the application of NO_3^- and NO_2^- as water purification technology. Upon extension of the reaction time, NH_2OH can be hydrogenated to NH_4^+ (eqn (5)) or disproportionate into NH_4^+ and nitrous oxide (N_2O, eqn (6)). The latter is quickly further hydrogenated into N_2 (eqn (7)).[24]

$$NH_2OH + H_2 + H^+ \rightarrow NH_4^+ + H_2O \qquad (5)$$

$$4\,NH_2OH + 2H^+ \rightarrow 2\,NH_4^+ + N_2O + 3H_2O \qquad (6)$$

$$N_2O + H_2 \rightarrow N_2 + H_2O \qquad (7)$$

Thus, NH_2OH is at least 50% decomposed into undesired NH_4^+. In previous research it was shown that NH_2OH decomposition proceeds exclusively *via* the hydrogenation pathway in the absence of NO_3^- and NO_2^- and in the presence of H_2 over a Pd/Al_2O_3 catalyst. In contrast, in the presence of residual NO_3^-, NO_2^- or their remaining surface species adsorbed on the catalyst, the hydrogenation and the disproportionation pathway contribute to the NH_2OH decomposition.[17]

In this study, NH_2OH is used as a reaction marker to unravel the interplay between the reaction rate of NO_2^- hydrogenation and the selectivity to NH_2OH, NH_4^+ and N_2. To do this we investigated detailed reaction kinetics for the NO_2^- hydrogenation on Pd/Al_2O_3 and SnPd/Al_2O_3 catalysts at different H_2 partial pressures, initial NO_2^- concentrations, and temperatures while monitoring the NH_2OH and NH_4^+ concentrations to deliver a complete picture of the selectivity patterns and reaction order dependencies. The results drastically change the prevailing view that ammonia and nitrogen are the only two reaction products while showcasing the complex interdependence between hydrogen, nitrite, and hydroxylamine ratios in the observed kinetics and product distribution.

2 Materials and methods

2.1 Materials

Pd/Al_2O_3 and Tin(II) chloride ($SnCl_2$) were purchased from Fisher Scientific and potassium nitrate (KNO_3), potassium nitrite (KNO_2), benzaldehyde ($\geq$99.5%), benzaldehyde oxime ($\geq$96.5%) and hydroxylamine (50 wt% in H_2O) were purchased from Sigma Aldrich.

2.2 Catalyst preparation

Pd/Al_2O_3 was dried before use and sieved to a support particle size <25 μm. SnPd/Al_2O_3 was prepared from the same Pd/Al_2O_3

(<25 μm) *via* controlled surface deposition.[25,26] Therefore, Pd/Al_2O_3 was suspended in water and exposed to a continuous gas flow of 80 : 10 : 10 mL min^{-1} H_2 : He : CO_2 to reduce the catalyst for 30 min at RT. $SnCl_2$ was dissolved in degassed Milli-Q water and a volume containing Sn in amounts corresponding to 40% of the monolayer capacity of Pd based on CO-chemisorption was added to the catalyst suspension. The suspension is stirred for another 30 min and subsequently filtered to recover the catalyst powder. The filter cake was dried in a vacuum at 70 °C followed by calcination (500 °C in 50 mL min^{-1} air, 5 °C min^{-1}, 5 h) and reduction (500 °C in 30 mL min^{-1} H_2 and N_2 each, 5 °C min^{-1}, 5 h) in a tube oven. The catalyst is stored in air at ambient temperature.

2.3 Catalyst characterization

The metal loadings were determined with X-ray fluorescence (XRF). For the measurements a Bruker S8 Tiger Series 1 4 kW X-ray spectrometer was used. The samples were measured as powder, in a sample cup with a Mylar film, in a helium environment. The concentrations of each element were calculated from the Kα or Lα lines of all elements, using the internal database. The metal dispersion and metal particle sizes were determined by CO-chemisorption. Therefore, the samples were reduced in H_2 for 1 h and purged with He for 20 min followed by CO-pulsing (all at RT, Micromeritics Chemisorb 2750). A Pd : CO 1 : 1 ratio and the geometry factor for a hemisphere (6) are assumed. The Brunauer–Emmet–Teller (BET) surface area was determined *via* N_2 physisorption at −196 °C after outgassing for 24 h at 300 °C (Micromeritics Tristar 3000). The characterization results are summarized in Table 1.

2.4 Catalytic testing

In a typical experiment, Pd/Al_2O_3 or SnPd/Al_2O_3 was suspended in 297 mL of deionized water in a 1 L baffled glass reactor equipped with a four-blade magnetic stirrer. The catalyst was reduced *in situ* under continuous gas flow (80 : 10 : 10 mL min^{-1} H_2 : CO_2 : He) for 1 h at 600 rpm. After the activation period, 3 mL of a KNO_2 stock solution was injected to reach the desired initial concentration and to initiate the reaction. Liquid samples were withdrawn periodically, passed through a 0.2 μm syringe filters to remove catalyst particles to terminate the reaction in the sample, and subsequently analyzed. NO_3^-, NO_2^- and NH_4^+ concentrations were analyzed *via* ion chromatography (IC, a Dionex ICS-3000 with electronic suppression, Thermo Fisher AS19 and CS12 columns with 20 mmol L^{-1} potassium hydroxide (KOH) and 20 mmol L^{-1} methane sulfonic acid (MSA) as eluents and an Automate 2000 autosampler). For NH_2OH determination, 0.5 μL benzaldehyde was added right after sampling to derivatize NH_2OH to benzaldehyde oxime.[17] Benzaldehyde oxime was quantified *via* HPLC (Shimadzu HPLC10AVP with an autosampler, a C18 hypersil gold column, a MeOH : H_2O (30 : 70 V% eluent, and a UV-vis detector at 248 nm). IC and HPLC analysis were conducted from the same sample vial and RT refers to 22 °C. In some experiments the analysis of the gas phase was attempted but ambient N_2 could not sufficiently be suppressed to ensure satisfactory sensitivity.

17238 | *J. Mater. Chem. A*, 2026, **14**, 17237–17249

This journal is © The Royal Society of Chemistry 2026

Table 1 Catalyst material properties based on N_2 physisorption, XRF and CO-chemisorption

Catalyst	BET surface area	Pd loading	Sn loading	Average Pd particle size
Pd/Al_2O_3	110 m^2 g^{-1}	8.1 wt%	—	10.3 nm
$SnPd/Al_2O_3$	—	8.4 wt%	0.7 wt%	—

In these approaches NO, NO_2 or N_2O could be detected. The selectivity was calculated as $S_{NH_4^+} = \dfrac{[NH_4^+]_t}{([NO_2^-]_0 - [NO_2^-]_t)}$ or $S_{NH_2OH} = \dfrac{[NH_2OH]_t}{([NO_2^-]_0 - [NO_2^-]_t)}$ and the remaining fraction to 1 considered as N_2.

3 Results and discussion

3.1 NO_2^- hydrogenation on Pd/Al_2O_3 at RT

The NO_2^- hydrogenation was conducted in a concentration window of 0.26–6.5 mmol L^{-1} at 0.8 bar H_2 and at H_2 partial pressures between 0.05 and 0.8 bar for 0.8 mmol L^{-1} NO_2^- in the absence of internal (SI, Fig. 1) and external mass transport limitations.[27,28] Initial rate constants were obtained from concentration–time profiles (SI, Fig. 2) and plotted in log–log form (Fig. 1) to determine the reaction orders. At RT, a reaction order close to zero with respect to NO_2^- and ~0.2 with respect to H_2 was observed, confirming previous results from our group.[27,28]

Thus, the NO_2^- hydrogenation activity at room temperature is independent of the NO_2^- concentration, while slightly accelerated by increasing H_2 partial pressure. The low sensitivity towards both NO_2^- and H_2 concentrations suggests that the catalyst surface is predominantly covered by intermediates prior to the rate-determining step, leaving few sites available for additional NO_2^- or H_2 adsorption. This interpretation is consistent with previous Attenuated Total Reflection Infrared Spectroscopy (ATR-IR) studies as discussed later.[29–31]

To evaluate the selectivity of the reaction, NH_4^+ and NH_2OH concentrations were measured delivering a typical reaction profile as shown in Fig. 2A. Initially both NH_4^+ and NH_2OH concentrations increase with decreasing NO_2^- concentration. While the NH_4^+ concentration consistently increases, the

NH_2OH concentration passes through a maximum and subsequently decreases illustrating its intermediary nature. The remaining part of the converted NO_2^- is assumed to be N_2. The NH_4^+ selectivity ranges from <1% to 10%, depending on the H_2 partial pressure and the NO_2^- conversion level. The NH_4^+ concentration increases at a faster rate when NO_2^- is near full conversion, reflecting shifts in surface coverages during the reaction. When plotted as a function of NO_2^- conversion, the NH_4^+ selectivity follows a U-shaped dependence (Fig. 2B). Before NO_2^- injection (i.e., at the start of the reaction), the catalyst is activated in H_2-saturated water, giving high surface H-coverage and a high H : N ratio, which promotes NH_4^+ formation. As the reaction proceeds, H-coverage decreases while N-coverage increases, favoring N–N coupling and thereby enhancing N_2 selectivity. At high NO_2^- conversion, N-species are depleted, the H : N ratio shifts back toward higher H-coverage, and NH_4^+ selectivity increases again. Thus, the time required to achieve a pseudo steady state is an intrinsic disadvantage of batch experiments due to their transient nature. The competitive adsorption of NO_2^- and H_2 was demonstrated by Postma et al.[32] and Huang et al.[28] but is often not considered in batch experiments. This highlights the importance of monitoring NH_4^+ selectivity over the entire conversion range, since relying on initial selectivity is likely biased by the initial high H-coverage. While NH_4^+ formation generally decreases with decreasing H_2 partial pressure, substantial NH_4^+ suppression occurs only under strongly H_2-deficient conditions (0.05 bar, Fig. 2B), which also reduces the NO_2^- hydrogenation rate. This dependence reflects the higher H_2 demand for NH_4^+ formation relative to NO_2^- hydrogenation (3 vs. 1.5 H_2 per NO_2^-, see eqn (2) and (3)).

Despite the intermediary character of NH_2OH, monitoring NH_2OH is crucial as its maximum concentration at RT is typically observed around full NO_2^- conversion (Fig. 1C), thus representing a point where the reaction could otherwise be
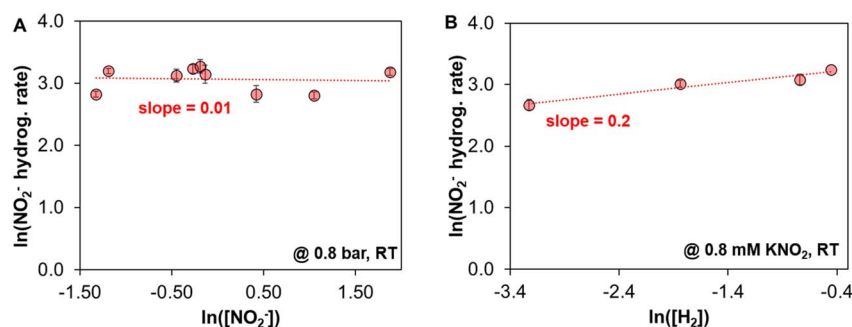

Fig. 1 Effect of NO_2^- (A) and H_2 concentration (B) on the NO_2^- hydrogenation rate on Pd/Al_2O_3. Reaction conditions: 300 mL H_2O, 0.3–6.5 mmol L^{-1} KNO_2, 10 mg Pd/Al_2O_3, 10 mL min^{-1} CO_2, 5–80 mL min^{-1} H_2 and He to balance to 100 mL min^{-1} total flow, RT, 600 rpm.

This journal is © The Royal Society of Chemistry 2026

J. Mater. Chem. A, 2026, **14**, 17237–17249 | **17239**

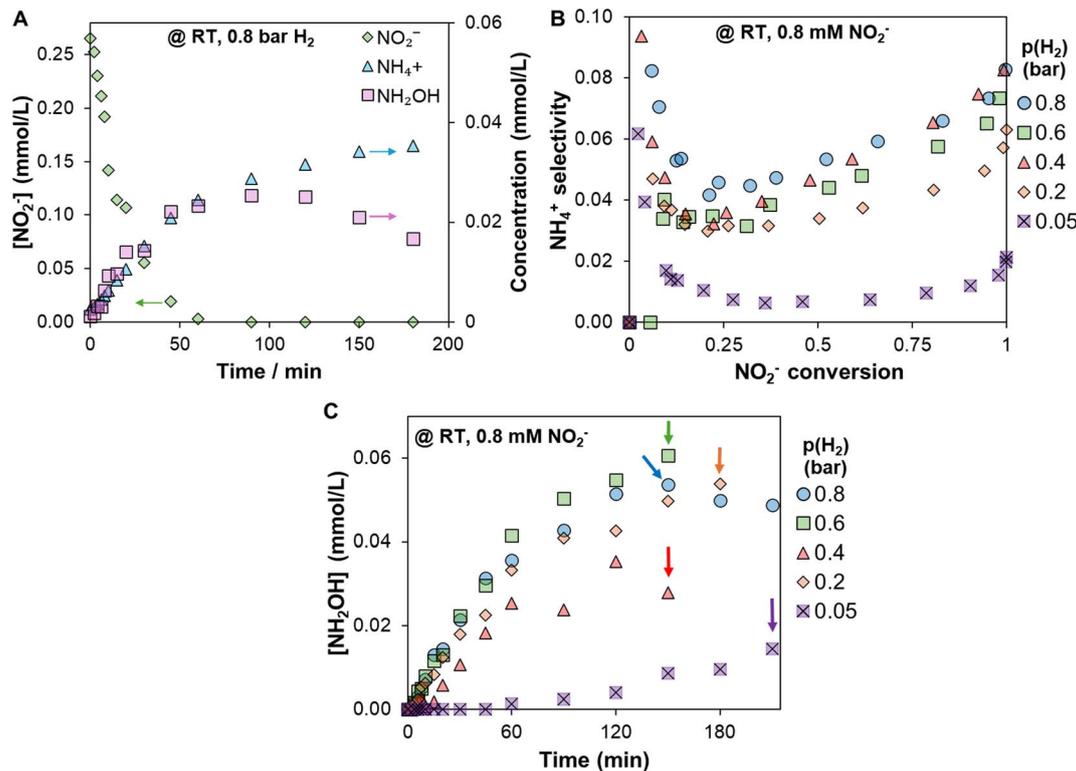**Fig. 2** Typical concentration profile of NO_2^- hydrogenation (A), NH_4^+ selectivity as a function of NO_2^- conversion (B) and NH_2OH concentration as a function of time in which arrows indicate full NO_2^- conversion (C). Reaction conditions: 300 mL H_2O, 10 mg Pd/Al_2O_3, 0.8 mmol L^{-1} KNO_2, 10 mL min^{-1} CO_2, 5–80 mL min^{-1} H_2 and He to balance to 100 mL min^{-1} total flow, RT, 600 rpm.

mistakenly considered complete. While the NH_2OH selectivity ranges from 3–8% at H_2 partial pressures ranging from 0.2 to 0.8 bar (SI, Fig. 3), the NH_2OH production is minimized when using very low H_2 partial pressure (0.05 bar, Fig. 2C). This drastic change in selectivity, however, comes at the expense of reduced NO_2^- hydrogenation. This behavior is consistent with the higher H_2 demand for NH_2OH formation compared to N_2 formation (2 *vs.* 1.5H_2 per NO_2^-, see eqn (2) and (4)).

Varying the initial NO_2^- concentration had little influence on NH_4^+ and NH_2OH formation (Fig. 3A and B, respectively) which is consistent with an apparent reaction order of zero in

NO_2^-, implying that the surface coverages are only mildly influenced by variation of the NO_2^- concentration. At the highest initial NO_2^- concentration, the formation of NH_4^+ and NH_2OH appears to be slightly reduced. This can be rationalized by increased N-coverage on the catalyst surface resulting in a higher N–N coupling probability which is in line with findings of Xu *et al.*[27]

3.2 NO_2^- hydrogenation on Pd/Al_2O_3 at 40 °C

The same set of experiments was performed at 40 °C to investigate the effect of reaction temperature. The H_2 reaction order
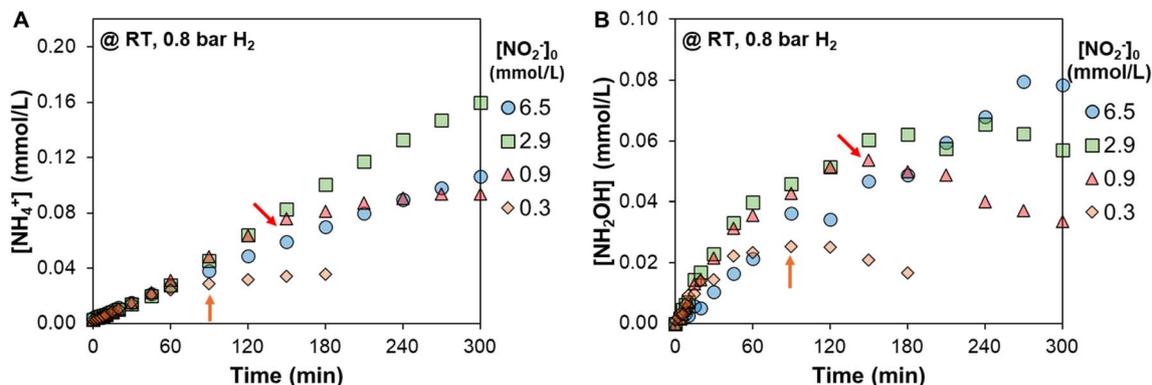

Fig. 3 NH_4^+ concentration (A) and NH_2OH concentration (B) at RT as a function of time at different initial NO_2^- concentrations. Arrows indicate the time of full NO_2^- conversion, if reached. Reaction conditions: 300 mL H_2O, 10 mg Pd/Al_2O_3, 80 : 10 : 10 mL min^{-1} H_2 : CO_2 : He, RT, 600 rpm.

remained ~0.2 while the NO_2^- hydrogenation activity is more sensitive to changes in the initial NO_2^- concentration at 40 °C illustrated by a positive reaction order of 0.24 below 0.8 mmol L^{-1} NO_2^- and a negative reaction order of −0.47 above 0.8 mmol L^{-1} (SI, Fig. 4).

A typical concentration profile at 40 °C is shown in the SI, Fig. 5. At 40 °C, the NH_4^+ selectivity increases from 3–8% (RT, Fig. 2B) to 10–15% or even to 25% (0.6 bar, Fig. 4A) and the U-shape is less pronounced, or at 0.6 bar even disappeared entirely. In contrast, the maximum NH_2OH concentration at 40 °C decreased by ~50% compared to RT and the maximum NH_2OH concentration is no longer observed near full NO_2^- conversion (Fig. 4B). Instead, the NH_2OH concentrations declined already before completion of NO_2^- hydrogenation. This indicates that elevated temperatures favor NH_2OH decomposition, lowering the measurable bulk NH_2OH concentration.

As NH_2OH primarily decomposes to NH_4^+, faster NH_2OH decomposition explains the higher NH_4^+ selectivity at 40 °C. Notably, the N_2 selectivity, calculated as the remainder of NH_4^+ and NH_2OH selectivity, is largely unchanged across most H_2 partial pressures at both RT and 40 °C (Fig. 4C). Thus, the additional NH_4^+ at 40 °C can be attributed to accelerated NH_2OH decomposition. Only at 0.6 bar of hydrogen the

nitrogen selectivity is substantially lower while NH_4^+ selectivity reaches a higher value, suggesting increased NH_4^+ formation from NO_2^-.

This kinetic study indicates that the formation of NH_4^+ can be suppressed under H_2-deficient conditions, albeit at the expense of lower overall NO_2^- hydrogenation rates. The selectivity toward NH_2OH depends on both hydrogen partial pressure and temperature. At low H_2 partial pressures, the selectivity to hydroxylamine is low due to hydrogen starvation on the catalyst surface, which limits its formation rate. With increasing temperature, NH_2OH selectivity also declines because of its accelerated decomposition to ammonia. This intricate interplay between surface coverage and activation barriers for hydroxylamine formation and decomposition highlights the inherent difficulty in controlling the selectivity toward hydroxylamine and ammonia in this reaction.

3.3 NO_2^- hydrogenation on Pd/Al_2O_3 with NH_2OH co-feeding

To evaluate the effect of NH_2OH on the selectivity and the NO_2^- hydrogenation activity, NH_2OH was co-fed in concentrations ranging from 0.1–0.85 mmol L^{-1} under H_2 deficient (0.05 bar) and H_2 rich (0.8 bar) conditions at both RT and 40 °C. As expected, higher NO_2^- hydrogenation rates were observed at
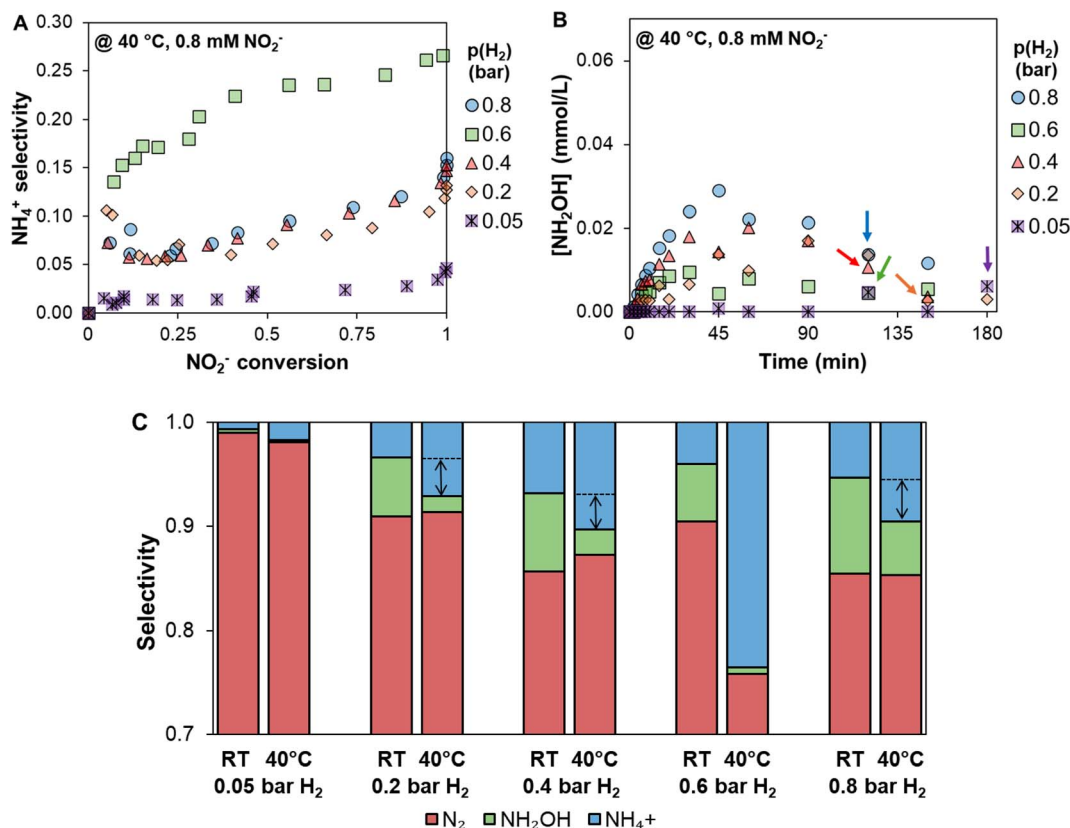

Fig. 4 NH_4^+ selectivity as a function of NO_2^- conversion (A), the NH_2OH concentration profile (B) both at 40 °C and selectivity distribution at ~50% NO_2^- conversion at RT and 40 °C and at different H_2 partial pressures (C). Arrows indicate full NO_2^- conversion (B) or the difference in NH_4^+ selectivity. Reaction conditions: 300 mL H_2O, 10 mg Pd/Al_2O_3, 0.8 mmol L^{-1} KNO_2, 10 mL min^{-1} CO_2, 5–80 mL min^{-1} H_2 and He to balance to 100 mL min^{-1} total flow, RT or 40 °C, 600 rpm.

This journal is © The Royal Society of Chemistry 2026

J. Mater. Chem. A, 2026, 14, 17237–17249 | 17241
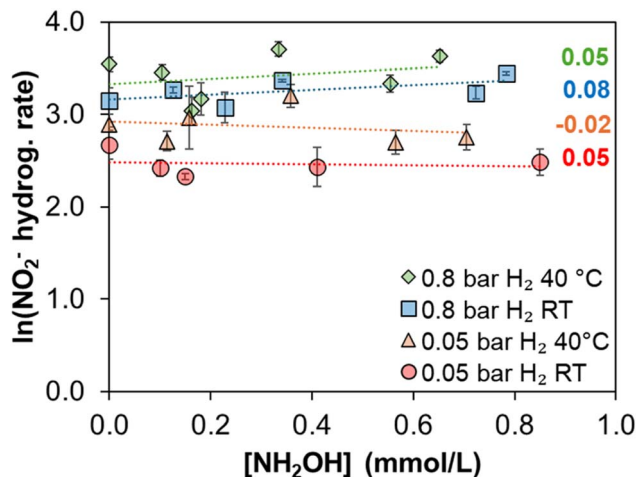
Fig. 5 Effect of NH$_2$OH on the NO$_2^-$ hydrogenation rate on Pd/Al$_2$O$_3$ at different H$_2$ partial pressures and different temperatures. Reaction conditions: 0.8 mmol L^{-1} KNO$_2$, 300 mL H$_2$O, 10 mg Pd/Al$_2$O$_3$, 10 mL min^{-1} CO$_2$, 5 or 80 mL min^{-1} H$_2$ and He to balance to 100 mL min^{-1} total flow, RT or 40 °C, 600 rpm.

elevated temperature and higher H$_2$ partial pressure. Surprisingly, the presence of co-fed NH$_2$OH did not affect the NO$_2^-$ hydrogenation activity regardless of temperature or H$_2$ partial pressure as illustrated by apparent reaction orders close to zero (Fig. 5).

Reporting the NH$_4^+$ and NH$_2$OH selectivity in NH$_2$OH co-feeding experiments is complex as co-fed NH$_2$OH represents an additional N-source resulting in an ill-defined denominator for the selectivity calculation. For instance, the NH$_2$OH selectivity could formally reach negative values and might therefore be misleading. To avoid this complexity, we report the NH$_4^+$ and NH$_2$OH concentrations as a function of time. Figures with the same data as a function of NO$_2^-$ conversion deliver the same trends and are shown in the SI, Fig. 6.

At RT, the NH$_2$OH concentration remained essentially constant at its initial co-feed level regardless of the H$_2$ partial pressure (Fig. 6A for 0.8 bar and SI, Fig. 6 for 0.05 bar). Because NH$_2$OH formation and decomposition occur simultaneously, only the net concentration change can be tracked. Thus, from the concentration profile alone, it cannot be determined whether NH$_2$OH formation and decomposition are in balance or whether no NH$_2$OH is formed in the first place. The NH$_4^+$ concentrations, however, increase with increasing NH$_2$OH co-feed at RT as illustrated by the first two clustered columns in Fig. 6D. This suggests that NH$_2$OH is not a passive spectator but NH$_2$OH formation and decomposition are in balance with the NH$_2$OH decomposition contributing to increased NH$_4^+$ formation. Under H$_2$-deficient conditions (0.05 bar), the NH$_4^+$ concentrations were consistently lower, as expected and discussed in Sections 3.1 and 3.2.

At 40 °C and low H$_2$ partial pressure the NH$_2$OH concentrations decrease over time resulting in slightly higher NH$_4^+$ concentrations (Fig. 6B and D (third clustered columns), respectively). The decrease in the NH$_2$OH concentration supports the earlier observations that the NH$_2$OH decomposition is promoted at elevated temperatures. At 40 °C and high H$_2$
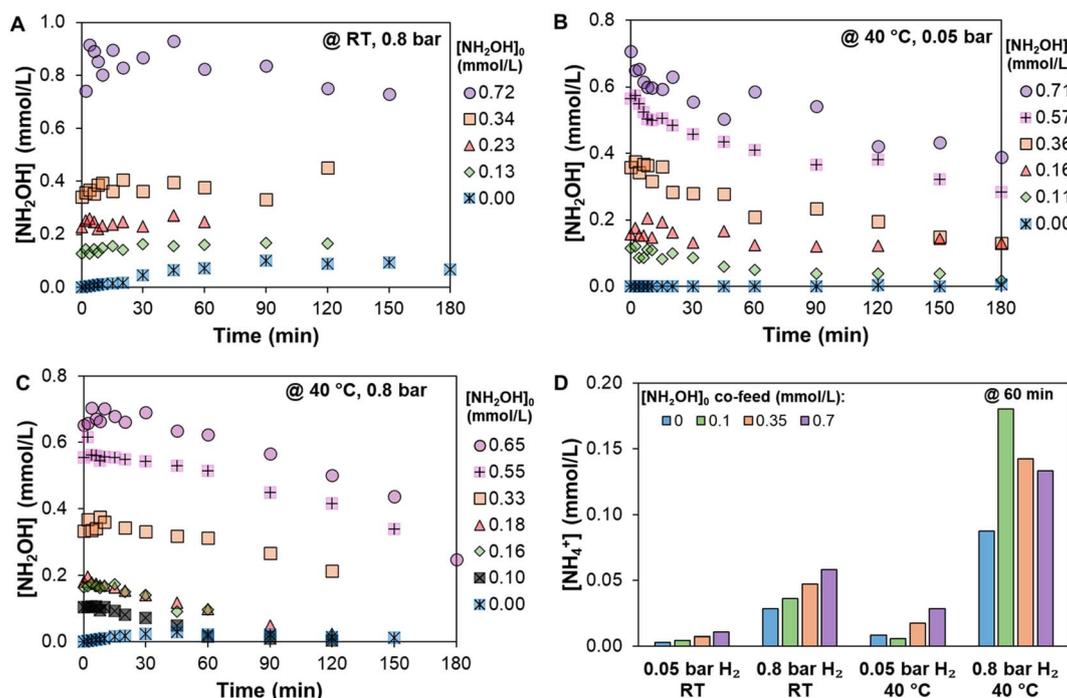
Fig. 6 NH$_2$OH concentration as a function of time at different NH$_2$OH co-feed concentrations at RT or 40 °C and at 0.8 or 0.05 bar H$_2$ (as stated in the chart, A–C) and the NH$_4^+$ concentration at different rounded NH$_2$OH co-feed concentrations after 60 min of reaction (D). Reaction conditions: 300 mL H$_2$O, 0.8 mmol L^{-1} KNO$_2$, 10 mg Pd/Al$_2$O$_3$, 80 or 5 mL min^{-1} H$_2$, 10 mL min^{-1} CO$_2$ and He to make up to 100 mL min^{-1}, RT or 40 °C, 600 rpm.

17242 | *J. Mater. Chem. A*, 2026, **14**, 17237–17249

This journal is © The Royal Society of Chemistry 2026

Table 2 Overview of the main trends of the NH_2OH co-feeding experiments with respect to NO_2^- hydrogenation activity, NH_2OH concentration and NH_4^+ formation under different reaction conditions

Effect of NH_2OH co-feeding	RT		40 °C	
	0.05 bar	0.8 bar	0.05 bar	0.8 bar
NO_2^- hydrog. activity			Activity unchanged	
$[NH_2OH]$	Constant		Decreasing	
NH_4^+ formation	Increasing with $[NH_2OH]_0$		Increased at high $[NH_2OH]_0$	Increasing non-linearly

partial pressure, substantially higher NH_4^+ concentrations are obtained than under all other conditions which underlines faster NH_2OH decomposition at elevated temperature and the need for sufficient H_2. Interestingly, the NH_4^+ concentrations show a non-linear behavior with respect to the NH_2OH co-feed levels under these conditions. While all co-feed experiments deliver higher NH_4^+ concentrations than the baseline experiment without any NH_2OH co-feed, the increase in the NH_4^+ concentration was more pronounced at lower co-feed levels (Fig. 6D, last clustered columns). A possible explanation could be that at high NH_2OH concentrations the surface is increasingly covered with NH_2OH species. This may result in lower H-coverage at high NH_2OH co-feed than at low NH_2OH co-feed leading to higher N : H ratios and therefore more N–N coupling and less NH_4^+ formation. More broadly, this underscores the complex interplay of the different surface species and its relevance for the reaction mechanism.

As summarized in Table 2, these findings indicate that the NO_2^- hydrogenation activity is unaffected by NH_2OH co-feeding. Instead, the hydroxylamine co-feeding led to higher NH_4^+ formation rates, indicating that this intermediate regulates the product selectivity. This increased NH_4^+ formation correlates with faster NH_2OH decomposition, which is more pronounced at elevated temperatures.

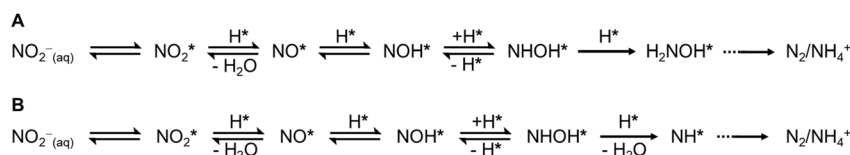## 3.4 Reviewing the NO_2^- hydrogenation reaction mechanism on Pd/Al_2O_3

Only very few studies propose a reaction mechanism considering elementary steps of the surface reaction and, to the best of our knowledge, none of them considers the desorption of NH_2OH.[27,28,33] Thus, earlier published mechanistically relevant findings based on ATR-IR spectroscopy,[29–31] DFT[28,33–35] and reaction kinetics[27,28] are critically discussed and a revised reaction mechanism under consideration of desorbed NH_2OH is provided. Mechanistic studies on NO_2^- over metals other than Pd[36] or NO_3^- hydrogenation[37–41] were not considered as the initial hydrogenation from NO_3^- to NO_2^- is the RDS of this

reaction and the surface coverages in NO_3^- and NO_2^- are thus not comparable.

3.4.1 Role of NH_2OH. Ebbesen *et al.* conducted ATR-IR studies on the decomposition of NH_2OH on Pd/Al_2O_3. They showed that in the absence of H_2 and NO_2^-, NH_2OH decomposes into NH_4^+ and another species that initially was assumed to be NH_2^*.[31] In following studies using isotope labelling, Rao *et al.* showed that this species contains oxygen and was therefore defined as NO_xH_y which represents HNO*, NOH*, NHOH* and/or NH_2OH^* (unpublished work, SI, Fig. 7). The three species were indistinguishable from one another. Subsequent titration of the $NO_xH_y^*$ species with H_2 in the ATR-IR cell showed that $NO_xH_y^*$ is converted into NH_4^+.[31] Notably, NO* was not observed in these experiments suggesting at least one irreversible reaction step from NO* towards $NO_xH_y^*$ on the Pd catalyst. In our latest work we reported NH_4^+ selectivity <100% in batch experiments converting NH_2OH. This indicates that N_2 or N_2O can be formed from NH_2OH even in the absence of NO_2^- and H_2 *via* catalytic disproportionation.[17] Generally, these results suggest that there is a direct pathway from NH_2OH towards NH_4^+, while NH_2OH can also merge into the mechanistic pathway that leads to N_2, but NH_2OH cannot form NO*.

3.4.2 Langmuir–Hinshelwood or Eley–Ridel mechanism for N_2 formation. Xu *et al.* formulated a NO_2^- hydrogenation mechanism based on extensive kinetic studies.[27] All possible Langmuir–Hinshelwood (LH) equations were derived and compared with the apparent reaction orders in a broad concentration regime. Four of these LH type reaction mechanisms match the observed reaction orders. Two of these mechanisms proceed *via* a N* species (see SI, Fig. 8C and D) and were excluded as earlier work of Zhao *et al.* claimed N* species to be kinetically irrelevant.[29] Zhao observed increasing NH_4^+ concentrations although NO_2^- was entirely converted and suggested N* as strongly adsorbed surface species that only very slowly converts into NH_4^+.[29] While this seemed a reasonable explanation as N* species are IR inactive and could therefore not be observed in ATR-IR studies, it cannot be excluded that

A

$$NO_2^-_{(aq)} \rightleftharpoons NO_2^* \xrightarrow[- H_2O]{H^*} NO^* \rightleftharpoons NOH^* \xrightarrow[- H^*]{+H^*} NHOH^* \xrightarrow{H^*} H_2NOH^* \cdots\!\!\longrightarrow N_2/NH_4^+$$

B

$$NO_2^-_{(aq)} \rightleftharpoons NO_2^* \xrightarrow[- H_2O]{H^*} NO^* \rightleftharpoons NOH^* \xrightarrow[- H^*]{+H^*} NHOH^* \xrightarrow[- H_2O]{H^*} NH^* \cdots\!\!\longrightarrow N_2/NH_4^+$$

Fig. 7 Suggested NO_2^- hydrogenation mechanisms by Xu *et al.*[27]

This journal is © The Royal Society of Chemistry 2026

J. Mater. Chem. A, 2026, **14**, 17237–17249 | **17243**

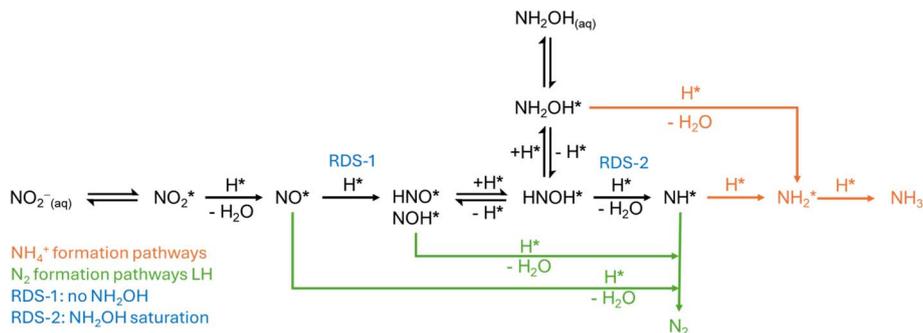**Fig. 8** Revised NO_2^- hydrogenation mechanism under consideration of NH_2OH desorption.

NH_2OH was formed in these experiments and the increase in the NH_4^+ concentration arose from NH_2OH decomposition. Nevertheless, DFT calculations showed that the N–O dissociation has a high activation barrier[28,34] and a high surface diffusion barrier of N*.[34] This disfavors the N* formation and subsequently reduces the probability of coupling with other surface species. Thus, N_2 formation based on a surface reaction pathway *via* N* appears unlikely.

Xu's two remaining mechanisms are shown in Fig. 7. The first one (A) was previously excluded based on ATR-IR results of Ebbesen *et al.*[31] that claim that NH_2OH cannot form N_2 since no N_2O* as an N_2 precursor was detected when feeding NH_2OH into the ATR-IR cell.[31] As mentioned, we observed NH_4^+ selectivity <100% in batch experiments converting NH_2OH indicating that N_2 can be formed from NH_2OH.[17] Thus, both mechanisms are an option based on the current knowledge. Huang *et al.* reported similar kinetic studies including micro-kinetic modelling and DFT calculations that consider proton shuttling effects of the solvent to further deepen the understanding of the reaction mechanism.[28] Essentially, the suggested reaction mechanism follows the same elementary steps as those reported by Xu *et al.*[27] shown in Fig. 7B.

In contrast to this LH-type mechanism, Lee *et al.* suggested an Elye Ridel (ER) like mechanism based on DFT in which N* reacts with H* and NO_2^- and H^+ from the liquid phase to form N_2O that is then quickly converted to N_2.[34]

$$N* + H* + NO_2^- + H^+ \rightarrow N_2O* + H_2O + * \qquad (8)$$
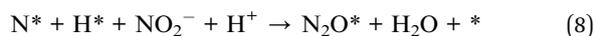
This reaction pathway is reported energetically favorable, but a reaction in which four molecules from two different phases meet and react in a concerted manner appears kinetically unlikely. Notably, this study did not consider transition state calculations so the authors themselves encourage careful interpretation of the suggested decomposition pathway.[34] While Wong *et al.*[33] adopt this EL mechanism, this elaboration will focus on the LH-type mechanism.

3.4.3 Revised NO_2^- hydrogenation mechanism: the N–N coupling pathway and RDS. Unraveling the exact coupling species is not realistically possible due to the complex interplay of different surface species which are to a great extent not even distinguishable (NO_xH_y). Nevertheless, we attempt to streamline the most probable reaction pathway, RDS and selectivity-

determining intermediates based on our experimental observations, ATR-IR findings, DFT calculations and reaction kinetics.

The suggested reaction pathway (Fig. 8) is inspired by the proposed mechanism by Xu *et al.*[27] as the results of the reaction kinetics experiments are similar in the studies by Xu *et al.*[27] and Huang *et al.*[28] and the present work. The revised version includes the desorption of NH_2OH that is evident due to the detection of NH_2OH species regardless of the reaction conditions.[17] Additionally, the hydrogenation equilibrium between NH_2OH* and $HNOH*$, which allows $NH_2OH_{(aq)}$ to merge into the N_2 formation pathway, is included. This is supported by NH_4^+ selectivity <100% in NH_2OH decomposition experiments[17] and represents a crucial difference with respect to the reaction mechanism suggested by Kim[34] and adopted by Wong.[33]

Under all investigated reaction conditions, N_2 was observed as the main product of the NO_2^- hydrogenation reaction. While N–N coupling is a prerequisite for N_2 formation, Xu *et al.*[27] demonstrated that this cannot be the rate determining step (RDS) of the reaction as the observed negative reaction orders at high NO_2^- concentrations and low H_2 partial pressures Xu observed do not match any rate expression considering N–N coupling. Instead, second order rate dependencies with respect to NO_2^- would have to be observed experimentally to support such N–N coupling as the RDS.[27] Direct coupling of surface abundant N-species ($NO*$ and $NO_xH_y^*$) can be rejected, since significant coupling of surface abundant species is intrinsically contradicting as the coverage would be drastically reduced as a consequence of their coupling. ATR-IR studies revealed the $NO*$ and the ill-defined $NO_xH_y^*$ species are surface abundant.[29–31] Thus, N_2 cannot be formed by NO–NO coupling, which is also supported by DFT calculations that suggest that dipole-repulsions between $NO*$ species would lead to high activation barriers.[34] The NH_2OH co-feeding experiments (Section 3.3) delivered zeroth order kinetics in NH_2OH; thus it is likely that the ill-defined surface abundant $NO_xH_y^*$ represents a highly hydrogenated species such as $HNOH*$ or NH_2OH*. Therefore, $HNOH*$ and NH_2OH* can also be excluded for coupling with itself or $NO*$ to produce N_2. Also, participation of N* in the N–N coupling is unlikely due to high surface diffusion barriers for N* as discussed in Section 3.4.2, leaving $NO*–NH*$, $NHO*–NH*$ or $NOH*–NH*$ as possible pathways for N_2 formation.

17244 | *J. Mater. Chem. A*, 2026, **14**, 17237–17249

This journal is © The Royal Society of Chemistry 2026

Huang et al.[28] suggested a co-limitation of the hydrogenation of NO* to HNO* and the consecutive hydrogenation of HNO* to HNOH* as the RDS based on their kinetic model.[28] DFT calculations in their work delivered lower activation barriers for HNOH* formation via HNO* than via NOH*. While NOH* might still form and couple with NH* to form N_2, we focus on HNO* for the subsequent pathway to HNOH*. Huang et al.[28] suggested that the degree of rate control shifts based on the reaction conditions but is under typical reaction conditions (RT, 0.8 bar H_2 partial pressure) at about 90% for the NO* hydrogenation to HNO*.

While the observed reaction kinetics in this work are similar and therefore confirm the previous model not considering NH_2OH, the model cannot explain the RDS in the presence of NH_2OH sufficiently. If NO* hydrogenation was also the dominant RDS under NH_2OH rich conditions, all following steps were quasi-equilibrated and thus $NH_2OH_{(aq)}$ was equilibrated with NH* according to the 0th law of thermodynamics. NH* can be coupled with NO* to form N_2 and NO* is easily formed from NO_2^- and surface abundant; thus an acceleration of the NO_2^- hydrogenation with increasing NH_2OH co-feed (NH_2OH reaction order > 0) would be expected. In other words, the NO* → NOH* RDS could be bypassed owing to the abundance of NH*. However, the observation is 0th order in NH_2OH; thus, there must be another RDS under NH_2OH rich conditions.

The H-assisted dissociation of the N–O bond in HNOH* to NH* can be a RDS based on the expected apparent reaction orders derived from the LH equations by Xu et al.[27] without considering NH_2OH. A similar derivation under NH_2OH rich conditions was derived (see the SI) and resulted in a reaction order range of [−1, 0] for NO_2^- and [−1, 1] for NH_2OH which covers the observed orders. Notably, in ATR-IR titration experiments of the surface abundant NO* and $NO_xH_y^*$ species it was observed that NO* is more quickly converted than $NO_xH_y^*$,[29,30] supporting that HNOH* → NH* is a realistic RDS.[24] Controversially, if HNOH* → NH* is the RDS under NH_2OH rich conditions, one might expect the reaction to be accelerated with increasing NH_2OH concentration due to increased HNOH* coverage. However, if the surface is saturated with NH_2OH (and its equilibrated species including HNOH*), changes in NH_2OH in the solution would not affect the reaction rate. This surface saturation of NH_2OH species under NH_2OH rich conditions agrees with ATR-IR experiments that showed that NH_xO_y is a surface abundant species when feeding NH_2OH.[30,31]

Thus, we suggest that the RDS varies even more on the surface coverages than reported by Huang et al.[28] In the absence of NH_2OH the RDS lies dominantly on the NO* → NOH* hydrogenation while it shifts to HNOH* → NH* under NH_2OH abundant conditions. In between these two extreme cases the degree of rate control shifts non-linearly and therefore accounts for intriguing trends such as decreasing NH_4^+ formation with increasing NH_2OH co-feed (Fig. 6D) or higher NH_4^+ formation at 0.6 bar H_2 and elevated temperature (Fig. 4C). NH* remains the last common reaction intermediate in the pathways towards N_2 and NH_4^+. Thus, the surface coverage of H* and various N* species determines the probability whether NH* proceeds via the N_2 or NH_4^+ pathway. Clearly, higher H-coverage increases the probability for NH_4^+ formation, which is consistent with increased NH_4^+ selectivity at the beginning of a reaction and approaching full NO_2^- conversion and lower NH_4^+ formation under H_2 deficient conditions as discussed in Section 3.1.

In conclusion, the recent discovery of NH_2OH as a desorbed reaction intermediate clearly highlights the need for the incorporation of NH_2OH into the NO_2^- hydrogenation mechanism. In our revised mechanistic scheme we (1) account for the adsorption equilibrium of NH_2OH, (2) include the hydrogenation equilibrium of HNOH* and NH_2OH^* representing the possibility for NH_2OH to merge into the N_2 formation pathway, and (3) suggest a changing degree of rate control depending on the surface coverages with NO hydrogenation as the dominant RDS in the absence of NH_2OH and the H-assisted N–O dissociation of HNOH* to NH* as the RDS under NH_2OH rich conditions. This mechanism emphasizes that the selectivity is determined by NH* conversion, either reacting with H* to form NH_4^+ or by coupling with an N-species to form N_2, depending on the surface coverage of H and HNO*/NOH* or NO*. Our proposed mechanism provides a coherent picture of the reaction mechanism consistent with the experimental data and previous results obtained from our group. Nonetheless, the dominant surface mechanism will inevitably depend on catalyst characteristics and operating conditions, and other mechanistic interpretations may also be reasonable.

3.5 NO_2^- hydrogenation on SnPd/Al_2O_3 – activity, selectivity and NH_2OH co-feeding

The same set of experiments, varying the NO_2^- concentration from 0.3–8 mmol L^{-1} and the H_2 partial pressure from 0.05–0.8 bar, was conducted on a SnPd/Al_2O_3 catalyst. This catalyst was prepared from the previously tested Pd/Al_2O_3 by Controlled Surface Deposition (CSD), introducing Sn corresponding to 0.4 monolayers relative to the accessible Pd surface atoms. Remarkably, the overall NO_2^- hydrogenation activity remained largely unaffected by Sn doping. Since the activity was unchanged, we assume, as for Pd/Al_2O_3, that mass transport limitations are absent (SI, Fig. 1). The derived reaction orders are likewise similar to those observed for Pd/Al_2O_3: the order in NO_2^- remains close to zero (Fig. 9A), while the order in H_2 increases from 0.2 (Pd/Al_2O_3) to 0.5 (SnPd/Al_2O_3, Fig. 9B), indicating a higher sensitivity to changes in H_2 partial pressure. This can be rationalized by the partial blockage of Pd sites by Sn, which cannot dissociate H_2, thereby reducing the effective H availability. In NH_2OH co-feeding experiments, the NO_2^- hydrogenation activity also remained unchanged, resulting in an apparent reaction order in NH_2OH close to zero at both 0.8 and 0.05 bar H_2 (Fig. 9C).

The selectivity trends on SnPd/Al_2O_3 mirror those on Pd/Al_2O_3: NH_2OH concentrations increase over the course of the reaction, peaking near full NO_2^- conversion (Fig. 10B), while NH_4^+ selectivity exhibits a U-shaped dependence on conversion (Fig. 10A) as discussed in Section 3.1. As for Pd/Al_2O_3, variations in the initial NO_2^- concentration have only minor effects on product distribution (SI, Fig. 9), and both NH_4^+ and NH_2OH
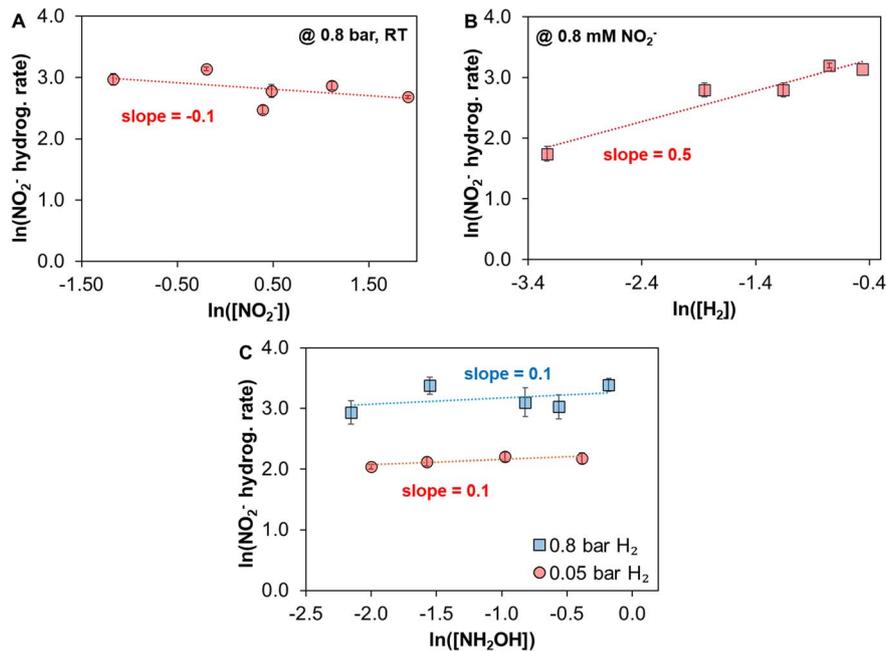
This journal is © The Royal Society of Chemistry 2026

J. Mater. Chem. A, 2026, **14**, 17237–17249 | **17245**

Fig. 9 Effect of NO_2^- (A), H_2 (B) and NH_2OH concentration (C) on the NO_2^- hydrogenation rate on $SnPd/Al_2O_3$. Reaction conditions: 300 mL H_2O, 10 mg $SnPd/Al_2O_3$, 10 mL min^{-1} CO_2, 5–80 mL min^{-1} H_2 and He to balance to 100 mL min^{-1} total flow, RT, 600 rpm.
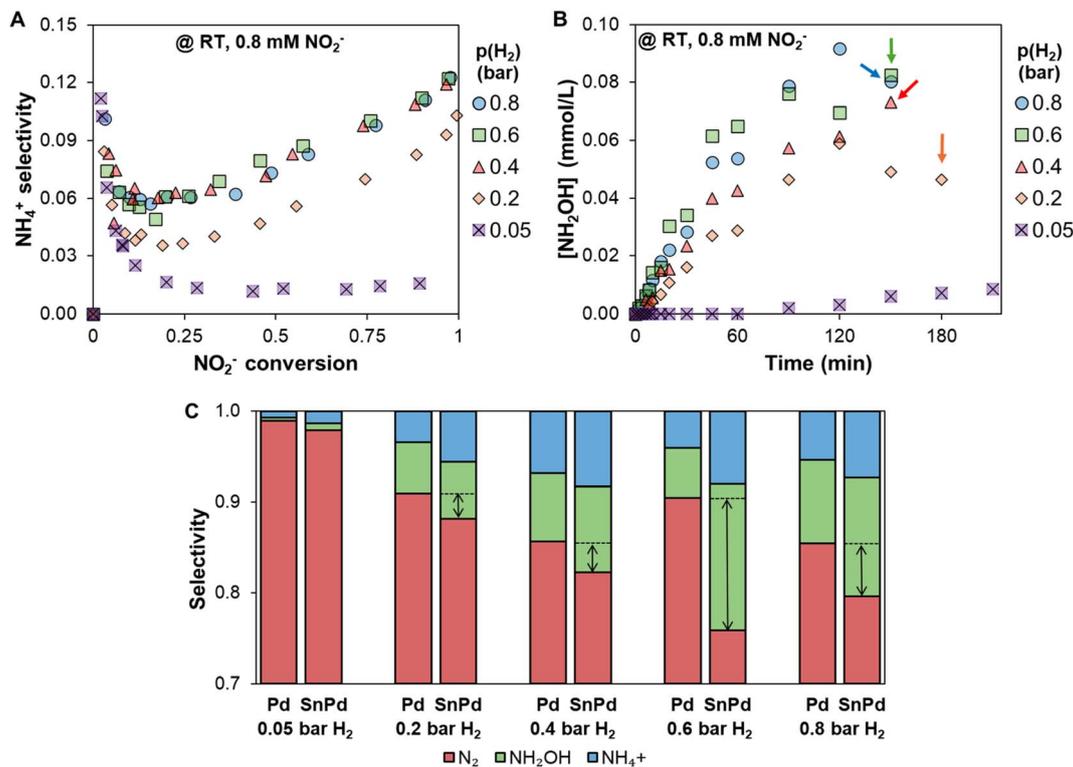

Fig. 10 NH_4^+ (A) and NH_2OH (B) concentrations as a function of NO_2^- conversion and time, respectively, and selectivity distribution at ~50% NO_2^- conversion on Pd and SnPd at different H_2 partial pressures (C). Pd data are the same as in Fig. 4 and replotted for intuitive comparison. The arrows in (C) indicate the difference in N_2 selectivity. Reaction conditions: 300 mL H_2O, 10 mg $SnPd/Al_2O_3$, 10 mL min^{-1} CO_2, 5–80 mL min^{-1} H_2 and He to balance to 100 mL min^{-1} total flow, RT or 40 °C, 600 rpm.

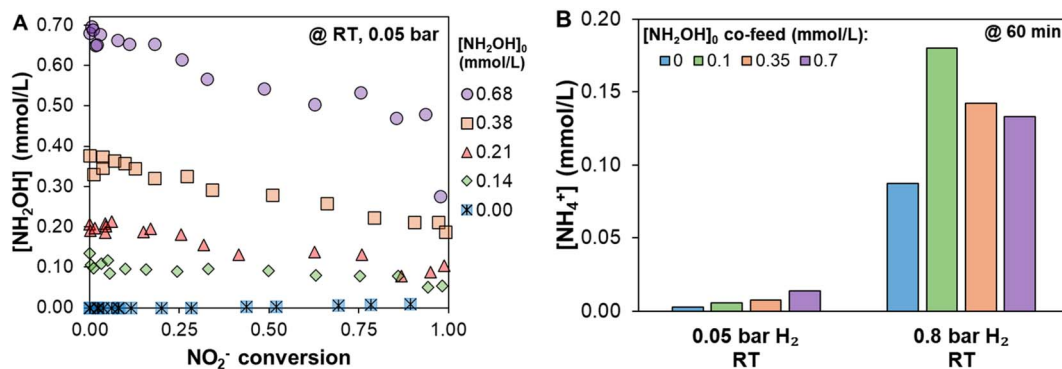**17246** | *J. Mater. Chem. A*, 2026, **14**, 17237–17249

This journal is © The Royal Society of Chemistry 2026

Fig. 11 NH_2OH concentration as a function of NO_2^- conversion at different NH_2OH co-feed concentrations at 0.05 bar H_2 (A) and the NH_4^+ concentration at different rounded NH_2OH co-feed concentrations after 60 min of reaction (B). Reaction conditions: 300 mL H_2O, 0.8 mmol L^{-1} KNO_2, 10 mg $SnPd/Al_2O_3$, 80 or 5 mL min^{-1} H_2, 10 mL min^{-1} CO_2 and He to make up to 100 mL min^{-1}, RT, 600 rpm.

concentrations are lower under H_2-deficient conditions (Fig. 10).

Notably, the NH_2OH and NH_4^+ selectivity are mildly increased on $SnPd/Al_2O_3$ for all H_2 pressures ≥ 0.2 bar resulting in 4–16% lower N_2 selectivity upon Sn doping (Fig. 10C). While this appears contradictory to the notion of reduced H coverage caused by Sn blocking of Pd sites, this suggests that Sn also shifts the balance of surface reactions away from N–N coupling and towards NH_4^+ formation. Formation of N_2 requires N–N bond formation *via* coupling between a reduced N adsorbate (*e.g.*, NH*) and a more oxidized N adsorbate (*e.g.*, NO*/NOH*/HNOH*), which therefore requires co-adsorption of these intermediates in close proximity on Pd ensembles. Introducing Sn partially dilutes Pd, reducing the probability for such coupling configurations and thus slightly suppressing the N_2 pathway.[42] In contrast, sequential hydrogenation steps toward NH_4^+ rely primarily on H* availability and are less sensitive to the availability of larger Pd ensembles.[42] This is consistent with the much higher mobility (lower diffusion barrier) of H* on Pd compared with N-species,[34] which favors hydrogenation when coupling upon Pd dilution. The same argumentation applies to NH_2OH formation, since it does not require N–N coupling but follows from stepwise hydrogenation. However, we cannot rule out that the presence of Sn modifies the electronic structure of neighboring Pd surface atoms, increasing the rate of hydrogenation to NH_4^+.

The NH_2OH co-feeding experiments at high H_2 partial pressure (0.8 bar) on $SnPd/Al_2O_3$ reproduce the trends observed on Pd/Al_2O_3: the NH_2OH concentration remains essentially constant, while more NH_4^+ is formed when NH_2OH is co-fed (SI, Fig. 10 and 11B). Interestingly, the same non-linearity is observed in decreasing NH_4^+ formation with increasing NH_2OH co-feed concentration, as on Pd at elevated temperature. Under H_2-deficient conditions, NH_2OH depletion is more pronounced on SnPd than on Pd (Fig. 11A and SI, Fig. 6F) and the NH_4^+ concentration increases with increasing NH_2OH co-feed concentration (Fig. 11B). The NH_2OH co-feeding results can be rationalized by the ability to disproportionate into NH_4^+ and N_2 without net consumption of H_2. Under H_2-deficient conditions this disproportionation pathway gains relative

importance, because pathways that rely on H_2 uptake are suppressed. On $SnPd/Al_2O_3$ this is more pronounced; thus the presence of Sn facilitates the NH_2OH decomposition. This is in line with the enhanced N–O bond activation ability of Sn also allowing to break the first N–O bond in NO_3^-. As a result, NH_2OH is more readily consumed on $SnPd/Al_2O_3$ than on Pd/Al_2O_3, consistent with the stronger decrease in the NH_2OH concentration observed at low H_2 partial pressure.

In conclusion, $SnPd/Al_2O_3$ exhibits NO_2^- hydrogenation activity and selectivity trends very similar to Pd/Al_2O_3. The main differences are a higher sensitivity to H_2 in both activity and selectivity, likely due to lower H affinity on SnPd. Also, the NH_2OH and NH_4^+ selectivities are increased resulting in a lower N_2 selectivity on SnPd.

In the bigger picture, these results show the demanding challenges for NO_3^- hydrogenation aiming for high N_2 selectivity. The NO_3^- hydrogenation requires a bimetallic catalyst such as $SnPd/Al_2O_3$ for the initial NO_3^- hydrogenation to NO_2^- which represents the RDS of this reaction. As a result, NO_2^- is commonly detected in traces or not detected in the liquid bulk at all. Thus, the surface coverage of N-species in the NO_3^- hydrogenation on the Pd sites is lower and shifts the coverage towards higher H : N ratios favoring NH_4^+ and NH_2OH formation. This in combination with the higher NH_4^+ production affinity of SnPd itself highlights the fundamental challenges of selective NO_3^- hydrogenation for drinking water purification.

4 Conclusion

In this study, we have demonstrated that NH_2OH is a key intermediate in the catalytic hydrogenation of NO_2^-. The selectivity towards NH_4^+ is strongly conversion-dependent, with both NH_2OH and NH_4^+ formation substantially suppressed only under H_2-deficient conditions, albeit at the expense of lower overall NO_2^- hydrogenation activity. Elevated temperature accelerates NH_2OH decomposition, thereby lowering the NH_2OH concentration. However, rather than enhancing N_2 formation, this shift promotes NH_4^+ selectivity leaving N_2 selectivity largely unaffected. Co-feeding experiments confirmed that the presence of NH_2OH does not influence the

This journal is © The Royal Society of Chemistry 2026

J. Mater. Chem. A, 2026, 14, 17237–17249 | 17247

intrinsic NO_2^- hydrogenation rate and that NH_2OH formation and decomposition are balanced. The latter suggests that a continuous process could in principle be designed in a way that NH_2OH would not excessively accumulate due to its intermediary nature. The activity and selectivity patterns for Pd/Al_2O_3 and $SnPd/Al_2O_3$ were very similar with higher NH_2OH and NH_4^+ formation on $SnPd/Al_2O_3$ being the main differences.

We critically reviewed the NO_2^- hydrogenation mechanism and provided a revised LH-based scheme including NH_2OH as desorbed species. The revised mechanism highlights that NH_2OH can merge into the N_2 formation pathway and suggests the RDS to be strongly dependent on the surface coverages.

Author contributions

J. Betting: methodology, investigation, writing – original draft; Y. Preedawichitkun: investigation; T. Sooknoi: funding acquisition, writing – review & editing; J. Faria Albanese: funding acquisition, supervision, writing – review & editing; L. Lefferts: supervision, writing – review & editing.

Conflicts of interest

There are no conflicts to declare.

Data availability

The data supporting this article have been included as part of the supplementary information (SI). Supplementary information is available. See DOI: https://doi.org/10.1039/d6ta00106h.

Acknowledgements

References

1 N. Lehnert, H. T. Dong, J. B. Harland, A. P. Hunt and C. J. White, *Nat. Rev. Chem.*, 2018, **2**, 278–289.

2 D. E. Canfield, A. N. Glazer and P. G. Falkowski, *Science*, 2010, **330**, 192–196.

3 X. Xia, S. Zhang, S. Li, L. Zhang, G. Wang, L. Zhang, J. Wang and Z. Li, *Environ Sci Process Impacts*, 2018, **20**, 863–891.

4 X. Zhang, B. B. Ward and D. M. Sigman, *Chem. Rev.*, 2020, **120**, 5308–5351.

5 M. Le Moal, C. Gascuel-Odoux, A. Ménesguen, Y. Souchon, C. Étrillard, A. Levain, F. Moatar, A. Pannard, P. Souchu, A. Lefebvre and G. Pinay, *Sci. Total Environ.*, 2019, **651**, 1–11.

6 C. S. Bruning-Fann and J. B. Kaneene, *Vet Hum Toxicol*, 1993, **35**, 521–538.

7 WHO, *Guidelines for Drinking-Water Quality*, 2022.

8 I. Sanchis, E. Diaz, A. H. Pizarro, J. J. Rodriguez and A. F. Mohedano, *Sep. Purif. Technol.*, 2022, **290**, 120750.

9 K. G. N. Quiton, M. C. Lu and Y. H. Huang, *Chemosphere*, 2021, **262**, 128371.

10 N. Barrabés and J. Sá, *Appl. Catal., B*, 2011, **104**, 1–5.

11 G. Tokazhanov, E. Ramazanova, S. Hamid, S. Bae and W. Lee, *Chem. Eng. J.*, 2020, **384**, 123252.

12 J. Martínez, A. Ortiz and I. Ortiz, *Appl. Catal., B*, 2017, **207**, 42–59.

13 European Union, *Directive on the Quality of Water Intended for Human Consumption*, 2020.

14 P. Liao, J. Kang, R. Xiang, S. Wang and G. Li, *Angew. Chem., Int. Ed.*, 2024, **63**, e202311752.

15 S. R. Udayasurian and T. Li, *Nanoscale*, 2024, **16**, 2805–2819.

16 C. L. Rooney, Q. Sun, B. Shang and H. Wang, *J. Am. Chem. Soc.*, 2025, **147**, 9378–9385.

17 J. Betting, L. Lefferts and J. Faria Albanese, *Chem. Commun.*, 2025, **61**, 12147–12150.

18 G. Yang, P. Zhou, J. Liang, H. Li and F. Wang, *Inorg. Chem. Front.*, 2023, **10**, 4610–4631.

19 G. Centi and S. Perathoner, *Appl. Catal., B*, 2003, **41**, 15–29.

20 V. I. Parvulescu, F. Epron, H. Garcia and P. Granger, *Chem. Rev.*, 2022, **122**, 2981–3121.

21 B. P. Chaplin, M. Reinhard, W. F. Schneider, C. Schüth, J. R. Shapley, T. J. Strathmann and C. J. Werth, *Environ. Sci. Technol.*, 2012, **46**, 3655–3670.

22 F. Ruiz-Beviá and M. J. Fernández-Torres, *J. Clean. Prod.*, 2019, **217**, 398–408.

23 European Commission, *Off. J. Eur. Union*, 2009, 207.

24 V. D. Moesdijk, *TU Eindhoven*, 1979.

25 A. Garron, K. Lázár and F. Epron, *Appl. Catal., B*, 2005, **59**, 57–69.

26 P. Munnik, P. E. De Jongh and K. P. De Jong, *Chem. Rev.*, 2015, **115**, 6687–6718.

27 P. Xu, S. Agarwal and L. Lefferts, *J. Catal.*, 2020, **383**, 124–134.

28 P. Huang, Y. Yan, A. Banerjee, L. Lefferts, B. Wang and J. A. Faria Albanese, *J. Catal.*, 2022, **413**, 252–263.

29 Y. Zhao, N. Koteswara Rao and L. Lefferts, *J. Catal.*, 2016, **337**, 102–110.

30 S. D. Ebbesen, B. L. Mojet and L. Lefferts, *J. Catal.*, 2008, **256**, 15–23.

31 S. D. Ebbesen, B. L. Mojet and L. Lefferts, *Langmuir*, 2008, **24**, 869–879.

32 R. S. Postma, R. Brunet Espinosa and L. Lefferts, *ChemCatChem*, 2018, **10**, 3770–3776.

33 H. Li, S. Guo, K. Shin, M. S. Wong and G. Henkelman, *ACS Catal.*, 2019, **9**, 7957–7966.

34 H. Shin, S. Jung, S. Bae, W. Lee and H. Kim, *Environ. Sci. Technol.*, 2014, **48**, 12768–12774.

35 L. Y. Huai, C. Z. He, H. Wang, H. Wen, W. C. Yi and J. Y. Liu, *J. Catal.*, 2015, **322**, 73–83.

36 C. A. Clark, C. P. Reddy, H. Xu, K. N. Heck, G. Luo, T. P. Senftle and M. S. Wong, *ACS Catal.*, 2020, **10**, 494–509.

37 S. Guo, K. Heck, S. Kasiraju, H. Qian, Z. Zhao, L. C. Grabow, J. T. Miller and M. S. Wong, *ACS Catal.*, 2018, **8**, 503–515.

38 U. Prüsse, M. Hähnlein, J. Daum and K.-D. Vorlop, *Catal. Today*, 2000, **55**, 79–90.

17248 | *J. Mater. Chem. A*, 2026, **14**, 17237–17249

This journal is © The Royal Society of Chemistry 2026

39 O. M. Ilinitch, L. V Nosova, V. V Gorodetskii, V. P. Ivanov, S. N. Trukhan, E. N. Gribov, S. V Bogdanov and F. P. Cuperus, *J. Mol. Catal. A Chem.*, 2000, **158**, 237–249.

40 J. Wärna, I. Turunen, T. Salmit and T. Maunula, *Chem. Eng. Sci.*, 1994, **49**, 5763–5773.

41 I. Mikami, Y. Sakamoto, Y. Yoshinaga and T. Okuhara, *Appl. Catal., B*, 2003, **44**, 79–86.

42 H. Berndt, I. Mönnich, B. Lücke and M. Menzel, *Tin Promoted Palladium Catalysts for Nitrate Removal from Drinking Water*, 2001, vol. 30.

This journal is © The Royal Society of Chemistry 2026

J. Mater. Chem. A, 2026, **14**, 17237–17249 | **17249**